**Luigi Bregant**
Department of Engineering and Architecture,
University of Trieste,
Via A. Valerio 10,
Trieste 34127, Italy
e-mail: bregant@units.it

**Lucia Parussini**
Department of Engineering and Architecture,
University of Trieste,
Via A. Valerio 10,
Trieste 34127, Italy
e-mail: lparussini@units.it

**Valentino Pediroda**
Department of Engineering and Architecture,
University of Trieste,
Via A. Valerio 10,
Trieste 34127, Italy
e-mail: pediroda@units.it

# Multifidelity Recursive Cokriging for Dynamic Systems' Response Modification

*In order to perform the accurate tuning of a machine and improve its performance to the requested tasks, the knowledge of the reciprocal influence among the system's parameters is of paramount importance to achieve the sought result with minimum effort and time. Numerical simulations are an invaluable tool to carry out the system optimization, but modeling limitations restrict the capabilities of this approach. On the other side, real tests and measurements are lengthy, expensive, and not always feasible. This is the reason why a mixed approach is presented in this work. The combination, through recursive cokriging, of low-fidelity, yet extensive, numerical model results, together with a limited number of highly accurate experimental measurements, allows to understand the dynamics of the machine in an extended and accurate way. The results of a controllable experiment are presented and the advantages and drawbacks of the proposed approach are also discussed.*

## 1 Introduction

In industrial practice, it is rarely possible to optimize all the system's parameters during the design phase or through simulation tools. Consequently, the system's tuning must inevitable be executed during the operative phase.

To this end, the possibility to combine experimentally acquired information and numerical models' results, to map the effects of different system's parameter setups, represents a clear competitive advantage in terms of process knowledge and faster system's tuning [1].

The focus of this work is to identify a system's natural frequencies, while varying its mass distribution, exploiting results from low-fidelity numerical models and high-fidelity experimental measurements. The motivation, underneath this test, is to predict the resonance frequencies of the system, as function of the masses' positions, minimizing the lengthy and expensive experimental-operational phases.

The adopted test case is rather simple, in order to have the total control of the system dynamics and validate the proposed approach. Of course, more interesting applications will be the tuning of complex machineries, where the number of variables explodes and the simulation models loose, inevitably, prediction capabilities and accuracy. Given the purpose, in this application, the system's natural frequencies can be simply identified both by experiment analysis, such as experimental modal analysis (EMA), and numerical analysis, such as finite element method (FEM). Both can be easily performed with good levels of reliability and the effort to detect how the natural frequencies vary changing the system setup is affordable. Clearly, as soon as the complexity of the system increases, this operation becomes extremely difficult and onerous, raising the number of setup configurations for which natural frequencies' values have to be acquired.

The classical approach to this issue, that is, the mapping of the effects of different system's parameter setups, would be to numerically compute the quantity of interest, changing the process parameters on a significant design of experiments (DOE). Furthermore, model updating approaches can be used to improve the numerical analysis results, enhancing the correlation between the measured data and the numerical models [2].

A different approach is based on the use of surrogate models of process parameters. Using these interpolating methods, it is possible to reduce the size of DOE on which the process parameters have to be actually simulated or measured. Most popular surrogate models are polynomial response surfaces, kriging, and artificial neural networks.

In literature, there are few examples where surrogate models are used for identifying plant characteristics starting from operative phase measurements [3]. An interesting work in this direction is presented in Ref. [4], where kriging is used to model the counter-electromotive force of an electric motor with rotor speed and position as input data. The kriging model, used in the mentioned work, is particularly interesting among the other surrogate models, because it allows not only to predict the unknown values of the quantity of interest, starting from a set of known values, but also to quantify the level of uncertainty associated with prediction. The development of kriging technique [5–7] has resulted in different forecasting methodologies, including cokriging, proposed by Kennedy and O'Hagan [8], where multiple information sources with different level of fidelity are exploited to estimate the surrogate model. Later, the Kennedy and O'Hagan model, has been reformulated by Gratiét et al. [9–11] as a recursive framework of *s*-independent kriging problems, known as recursive cokriging. In this approach, a sequence of simpler kriging problems has to be solved, with smaller covariance matrices when compared with the original Kennedy and O'Hagan formulation.

The recursive cokriging model not only has the interesting feature to associate an error estimation of the predicted model, as standard kriging, but also allows a more efficient handling of the information sources' reliability with respect to cokriging. These properties make the recursive cokriging very attractive to build a response surface of process parameters during the operative phase.

In this work, the updated model computed by FEM, and both kriging and recursive cokriging models are compared on their capability of mapping the process variable influences and to provide simplified and faster tuning processes.

The paper is organized as follows: Section 2 introduces the kriging and recursive cokriging theory. In Sec. 3, the test case used to compare the updated model, kriging, and recursive cokriging is described. Section 4 illustrates the results obtained. Section 5 reports an application. Finally, in Sec. 6, our main findings are discussed.

## 2 Kriging and Recursive Cokriging Theory

**2.1 Kriging.** In kriging theory, the response $z(\mathbf{x})$, which is a deterministic real-valued function of the $d$-dimensional variable $\mathbf{x} = (x_1,\ldots, x_d)$, is considered as a realization of a Gaussian process $Z(\mathbf{x})$. $Z(\mathbf{x})$ is assumed to be the sum of a deterministic regression function $m(\mathbf{x})$, constructed by observed data, and a Gaussian process $Y(\mathbf{x})$, constructed through the residuals

$$Z(\mathbf{x}) = m(\mathbf{x}) + Y(\mathbf{x}) \tag{1}$$

The trend function $m(\mathbf{x})$ is actually the mean of the broader Gaussian process $Z(\mathbf{x})$, and it is assumed to be a multivariate polynomial, namely, $m(\mathbf{x}) = \mathbf{h}(\mathbf{x})\,\boldsymbol{\beta}$, where $\mathbf{h}(\mathbf{x})$ is a vector of polynomial basis functions and $\boldsymbol{\beta}$ is the vector of coefficients. $Y(\mathbf{x})$ is the Gaussian process with zero mean and covariance function $C(\mathbf{x}, \mathbf{x}') = \sigma^2 r(\mathbf{x}, \mathbf{x}'; \boldsymbol{\theta})$, where $\sigma^2$ is a scale parameter, called the process variance, and $r$ is a positive function with parameters $\boldsymbol{\theta}$, called the correlation function.

Let us suppose that $z(\mathbf{x})$ has been evaluated at a set of $n$ samples $\mathcal{D} = (\mathbf{x}_1, \ldots, \mathbf{x}_n)^{\mathrm{T}}$. We denote by $\mathbf{Z}^{(n)} = (Z_1, \ldots, Z_n)^{\mathrm{T}}$ the Gaussian vector containing the values of the random process $Z(\mathbf{x})$ at the points in the experimental design set $\mathcal{D}$ and by $\mathbf{z}^{(n)} = (z_1, \ldots, z_n)^{\mathrm{T}}$ the vector containing the values of $z(\mathbf{x})$ at the points in $\mathcal{D}$.

We use the information contained in $\mathbf{Z}^{(n)}$ to predict $Z(\mathbf{x})$ considering the joint distribution of $Z(\mathbf{x})$ and $\mathbf{Z}^{(n)}$. Then, the conditional distribution $[Z(\mathbf{x})|\mathbf{Z}^{(n)} = \mathbf{z}^{(n)}, \boldsymbol{\beta}, \sigma^2, \boldsymbol{\theta}]$ is a Gaussian $\mathcal{N}(\hat{m}_Z(\mathbf{x}), \hat{s}_Z^2(\mathbf{x}))$ with

$$\hat{m}_Z(\mathbf{x}) = \mathbf{h}(\mathbf{x})\boldsymbol{\beta} + \mathbf{r}^{\mathrm{T}}(\mathbf{x})\mathbf{R}^{-1}(\mathbf{z}^{(n)} - \mathbf{H}\boldsymbol{\beta}) \tag{2}$$

and

$$\hat{s}_Z^2(\mathbf{x}) = \sigma^2(1 - \mathbf{r}^{\mathrm{T}}(\mathbf{x})\mathbf{R}^{-1}\mathbf{r}(\mathbf{x})) \tag{3}$$

where $\mathbf{H}$ is the model matrix, $\mathbf{R}$ is the correlation matrix between the observations $\mathbf{Z}^{(n)}$, $\mathbf{r}(\mathbf{x})$ is the correlation vector between $Z(\mathbf{x})$ and the observations $\mathbf{Z}^{(n)}$, and $\boldsymbol{\beta}$ is evaluated as $\boldsymbol{\beta} = (\mathbf{H}^{\mathrm{T}}\mathbf{R}^{-1}\mathbf{H})^{-1}\mathbf{H}^{\mathrm{T}}\mathbf{R}^{-1}\mathbf{z}^{(n)}$ (see Appendix A). The hyperparameters $\boldsymbol{\theta}$ of the correlation function $r$ are identified by the maximum likelihood estimation, so that the process variance $\sigma^2 = (1/n)(\mathbf{z}^{(n)} - \mathbf{H}\boldsymbol{\beta})^{\mathrm{T}}\mathbf{R}^{-1}(\mathbf{z}^{(n)} - \mathbf{H}\boldsymbol{\beta})$ is the maximum likelihood estimate for $\sigma^2$ given $\boldsymbol{\beta}$.

In Eqs. (2) and (3), $\hat{m}_Z(\mathbf{x})$ is the kriging mean, which is the surrogate model that we use to approximate the response $z(\mathbf{x})$, and $\hat{s}_Z^2(\mathbf{x})$ is the kriging variance, which represents the model mean squared error.

**2.2 Recursive Cokriging.** Recursive cokriging is a recursive framework of $s$ independent kriging problems, which exploits multifidelity data coming from sources with different reliability.

In this case, there are $s$ levels of response $(z_t(\mathbf{x}))_{t=1,\ldots,s}$ sorted by increasing order of fidelity and modeled by Gaussian processes $(Z_t(\mathbf{x}))_{t=1,\ldots,s}$, $\mathbf{x} \in \mathcal{X}$. $z_s(\mathbf{x})$ is the most accurate and costly response and $(z_t(\mathbf{x}))_{t=1,\ldots,s-1}$ are cheaper versions of it, with $z_1(\mathbf{x})$ the less accurate one.

An autoregressive model can be formulated for $t = 2,\ldots, s$

$$\begin{cases} Z_t(\mathbf{x}) = \rho_{t-1}(\mathbf{x})Z_{t-1}(\mathbf{x}) + \delta_t(\mathbf{x}) \\ Z_{t-1}(\mathbf{x}) \perp \delta_t(\mathbf{x}) \\ \rho_{t-1}(\mathbf{x}) = \mathbf{g}_{t-1}^{T}(\mathbf{x})\boldsymbol{\beta}_{\rho_{t-1}} \end{cases} \tag{4}$$

where $\delta_t(\mathbf{x})$ is a Gaussian process, with mean $\mathbf{f}_t^{\mathrm{T}}(\mathbf{x})\boldsymbol{\beta}_t$ and covariance function $\sigma_t^2 r_t(\mathbf{x}, \mathbf{x}')$, independent of $Z_{t-1}(\mathbf{x}), \ldots, Z_1(\mathbf{x})$ and $\rho_{t-1}(\mathbf{x})$ represents a scale factor between $Z_t(\mathbf{x})$ and $Z_{t-1}(\mathbf{x})$. $\mathbf{g}_{t-1}(\mathbf{x})$ and $\mathbf{f}_t(\mathbf{x})$ are vectors of polynomial basis functions and $\boldsymbol{\beta}_{\rho_{t-1}}$ and $\boldsymbol{\beta}_t$ are the vectors of coefficients.

The Gaussian process $Z_t(\mathbf{x})$ modeling the response at level $t$ is expressed as a function of the Gaussian process $Z_{t-1}(\mathbf{x})$ conditioned by the values $\mathbf{z}^{(t-1)} = (\mathbf{z}_1, \ldots, \mathbf{z}_{t-1})$ at points in the experimental design sets $(\mathcal{D}_i)_{i=1,\ldots,t-1}$.

We have for $t = 2,\ldots, s$ and for $\mathbf{x} \in \mathcal{X}$

$$[Z_t(\mathbf{x})|\mathbf{Z}^{(t)} = \mathbf{z}^{(t)}, \boldsymbol{\beta}_t, \boldsymbol{\beta}_{\rho_{t-1}}, \sigma_t^2] \sim \mathcal{N}(\hat{m}_{Z_t}(\mathbf{x}), \hat{s}_{Z_t}^2(\mathbf{x})) \tag{5}$$

where

$$\begin{aligned} \hat{m}_{Z_t}(\mathbf{x}) = {} & \rho_{t-1}(\mathbf{x})\hat{m}_{Z_{t-1}}(\mathbf{x}) + \mathbf{f}_t^{\mathrm{T}}(\mathbf{x})\boldsymbol{\beta}_t \\ & + \mathbf{r}_t^{\mathrm{T}}(\mathbf{x})\mathbf{R}_t^{-1}(\mathbf{z}_t - \rho_{t-1}(\mathcal{D}_t) \odot \mathbf{z}_{t-1}(\mathcal{D}_t) - \mathbf{F}_t\boldsymbol{\beta}_t) \end{aligned} \tag{6}$$

and

$$\hat{s}_{Z_t}^2(\mathbf{x}) = \rho_{t-1}^2(\mathbf{x})\hat{s}_{Z_{t-1}}^2(\mathbf{x}) + \sigma_t^2(1 - \mathbf{r}_t^{\mathrm{T}}(\mathbf{x})\mathbf{R}_t^{-1}\mathbf{r}_t(\mathbf{x})) \tag{7}$$

The notation $\odot$ represents the Hadamard product. $\mathbf{R}_t$ is the correlation matrix and $\mathbf{r}_t^{\mathrm{T}}(\mathbf{x})$ is the correlation vector. We denote by $\rho_{t-1}(\mathcal{D}_t)$ the vector containing the values of $\rho_{t-1}(\mathbf{x})$ for $\mathbf{x} \in \mathcal{D}_t$, $\mathbf{z}_{t-1}(\mathcal{D}_t)$ the vector containing the known values of $Z_t(\mathbf{x})$ at points in $\mathcal{D}_t$, and $\mathbf{F}_t$ is the experience matrix containing the values of $\mathbf{f}_t(\mathbf{x})^{\mathrm{T}}$ on $\mathcal{D}_t$ (see Appendix B).

The recursive framework of cokriging is clearly visible in Eqs. (6) and (7), where the mean and the variance of the Gaussian process $Z_t(\mathbf{x})$ are functions of mean and variance of the Gaussian process $Z_{t-1}(\mathbf{x})$.

The mean $\hat{\mu}_{Z_t}(\mathbf{x})$ is the surrogate model of the response at level $t$, $1 \le t \le s$, taking into account the known values of the $t$ first levels of responses $(\mathbf{z}_i)_{i=1,\ldots,t}$. The variance $\hat{s}_{Z_t}^2(\mathbf{x})$ represents the mean squared error of the surrogate model of the response at level $t$. The variance will be zero at known values of the $t$ first levels of responses.

The parameters $(\boldsymbol{\theta}_t)$ are estimated by minimizing the opposite of the concentrated restricted log-likelihoods at each level $t$

$$\log(|\det(\mathbf{R}_t)|) + (n_t - p_t - q_{t-1})\log(\hat{\sigma}_t^2) \tag{8}$$

for $t = 1,\ldots, s$.

## 3 Test Case

The analyzed test case is a simple system, in order to have complete control on the variables and measurements and to have an easier three dimensional representation of the analysis results. We are aware that caution is needed to extend the achieved conclusions to more complex systems. In these latter case, the number of variables and their combinations will lead to very large solution spaces, with very high computational and time costs to be fully explored. In most cases, it could become prohibitive for plant requirements, and this is the reason why nowadays, the tuning is mostly done on the base of previous experiences and good sense. Nevertheless, we believe that the obtained results are meaningful and a proof of correctness of the proposed approach.

We consider a rectangular steel plate, on which two masses can be added to change the system's mass distribution. The system is shown in Fig. 1. For easiness of results representation, the two masses are placed along two lines, parallel to the long side on the plate, at fixed ordinates. The different positions of the masses, $(x_1, y_1)$ for mass 1 and $(x_2, y_2)$ for mass 2, represent the specific setup configuration. As $y_1$ and $y_2$ are constant, a configuration is completely described by two variables, $x_1$ and $x_2$.

The goal is to identify the natural frequencies of the system for all the possible configurations $(x_1, x_2) \in [80, 480] \times [300, 500]$ mm$^2$. Only the first 10 system's natural frequencies have been considered in the present analysis.

The natural frequencies values have been experimentally evaluated for 11 different masses' configurations. Three configurations of these, henceforth named as test points, $p_1$, $p_2$, and $p_3$,

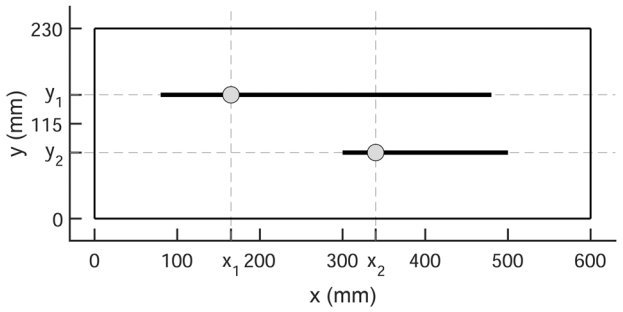


**Fig. 1 Scheme of test system (bold lines represent the locus of points where the two masses can be positioned)**

**Table 1 List of the three configurations used as test points**

| (mm) | $p_1$ | $p_2$ | $p_3$ |
|---|---|---|---|
| $x_1$ | 180 | 180 | 300 |
| $x_2$ | 300 | 420 | 300 |

have been used to analyze the methodologies (see Table 1 for the coordinates ($x_1$, $x_2$) of test points), the remaining have been used as training points for the model updating and the building of response surfaces. As an example, the experimental values of natural frequency 9 are shown in Fig. 2(*a*). In Table 2, the values of the first 10 natural frequencies in the test points are reported.

The natural frequencies' values have been obtained by an FEM numerical model, too. We have computed them for 2500 different configurations. Figure 2(*b*) shows the numerical values of natural frequency 9, computed by FEM code with a fine mesh, as function of the position of the masses along the coordinates $x_1$ and $x_2$. The nodes of the mesh plotted in figure correspond to computed values of natural frequencies. A subset of the natural frequencies' values computed by FEM code has been used for training the low-fidelity level of cokriging surface. More details are given in Secs. 3.1 and 3.2.

**3.1 Experimental Setup.** The transfer function measurements and the subsequent natural frequencies identification were carried out using an LMS Pimento data acquisition and analysis system.

The structure used in the experiment is 600 mm by 230 mm by 1 mm plate on which two extra masses, of about 30 g, have been

**Table 2 The first 10 EMA natural frequencies *f* in test points**

| (Hz) | $p_1$ | $p_2$ | $p_3$ |
|---|---|---|---|
| $f_1$ | 28.32 | 28.81 | 27.95 |
| $f_2$ | 46.75 | 46.51 | 46.88 |
| $f_3$ | 78.37 | 77.15 | 80.08 |
| $f_4$ | 98.51 | 99.61 | 98.02 |
| $f_5$ | 151.49 | 152.71 | 149.66 |
| $f_6$ | 161.13 | 160.28 | 162.35 |
| $f_7$ | 199.22 | 198.12 | 200.44 |
| $f_8$ | 218.26 | 216.55 | 220.09 |
| $f_9$ | 241.33 | 242.43 | 240.36 |
| $f_{10}$ | 260.62 | 260.99 | 261.11 |

added through small neodymium magnets. These can move along two ordinates, $y_1 = 150$ mm for mass 1 and $y_2 = 80$ mm for mass 2. The plate was suspended through very soft springs along the shortest side, in order to simulate free–free boundary conditions. These have been achieved assuring a sufficient separation between the last rigid mode (suspension) and the first flexible mode (plate).

The measurement have been acquired using a rowing hammer technique (PCB Modal Hammer 086C01) on ten degrees-of-freedom evenly distributed on the plate. Great care have been devoted to minimize the disturbance caused by sensors (PCB 352C22 0.5 g) and to select the best acquisition parameters to increase the frequency response function frequency resolution (0.05 Hz) and improve the overall quality of the measurements.

**3.2 Finite Element Method Model.** The plate and the added masses have been modeled in ANSYS APDL. The implemented Block Lanczos natural frequency and mode shape extraction method has been used between 0 and 1000 Hz. The added masses were both modeled as accurate geometries or as point masses without leading to relevant discrepancies.

First, the only plate vibrational modes have been simulated using Young's modulus $E = 210{,}000$ N/mm$^2$ and density $\rho = 7800$ kg/m$^3$. No additional masses have been simulated. The mesh size have been changed between 50 and 1 mm in order to simulate the dynamics of the simplified system with different levels of approximation. The results of convergence analysis are reported in Table 3 together with the experimental values of natural frequencies of the plate without masses.

Later, the natural frequencies of the complete system, plate and masses, have been computed for 2500 different configurations using mesh size equal to 10 mm, henceforth named coarse mesh

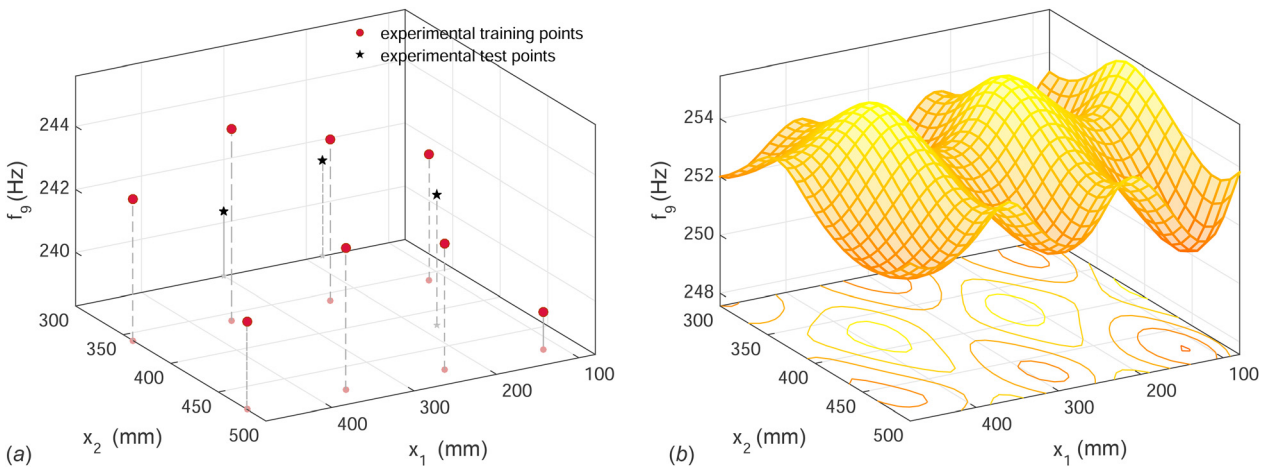


**Fig. 2 Natural frequency 9 for different configurations of masses ($x_1$, $x_2$): (*a*) values measured for 11 different configurations ($x_1$, $x_2$) and (*b*) values computed by FEM code with the fine mesh in 2500 different configurations ($x_1$, $x_2$)**

**Table 3 Convergence analysis of the first 10 natural frequencies *f* of the plate; the EMA values are reported for comparison**

| | | Mesh size (mm) | | | | | |
|---|---|---|---|---|---|---|---|
| (Hz) | Experimental | 50 | 30 | 10 | 5 | 3 | 1 |
| $f_1$ | 28.93 | 30.09 | 29.89 | 29.79 | 29.78 | 29.78 | 29.78 |
| $f_2$ | 46.88 | 47.90 | 47.78 | 47.71 | 47.68 | 47.65 | 47.61 |
| $f_3$ | 80.18 | 86.03 | 83.93 | 82.88 | 82.78 | 82.76 | 82.74 |
| $f_4$ | 99.61 | 103.41 | 102.52 | 102.02 | 101.93 | 101.87 | 101.78 |
| $f_5$ | 156.62 | 174.60 | 167.07 | 162.74 | 162.33 | 162.24 | 162.18 |
| $f_6$ | 162.23 | 175.88 | 171.24 | 169.48 | 169.24 | 169.12 | 168.97 |
| $f_7$ | 202.64 | 224.16 | 216.34 | 211.75 | 211.27 | 211.17 | 211.11 |
| $f_8$ | 220.58 | 240.30 | 233.07 | 228.64 | 228.14 | 228.00 | 227.89 |
| $f_9$ | 245.48 | 271.31 | 261.20 | 256.05 | 255.45 | 255.25 | 255.02 |
| $f_{10}$ | 262.82 | 303.41 | 290.21 | 276.91 | 275.68 | 275.40 | 275.25 |

**Table 4 Absolute errors of FEM model respect to experimental natural frequencies in test points**

| | Fine mesh | | | Coarse mesh | | |
|---|---|---|---|---|---|---|
| (Hz) | $p_1$ | $p_2$ | $p_3$ | $p_1$ | $p_2$ | $p_3$ |
| $E_1$ | 0.87 | 0.78 | 0.86 | 0.88 | 0.79 | 0.87 |
| $E_2$ | 0.82 | 0.96 | 0.80 | 0.85 | 0.99 | 0.83 |
| $E_3$ | 2.82 | 2.51 | 2.70 | 2.92 | 2.60 | 2.80 |
| $E_4$ | 2.64 | 2.18 | 2.54 | 2.73 | 2.27 | 2.63 |
| $E_5$ | 5.97 | 7.42 | 5.04 | 6.36 | 7.81 | 5.41 |
| $E_6$ | 7.07 | 7.21 | 6.89 | 7.31 | 7.46 | 7.13 |
| $E_7$ | 8.47 | 8.40 | 9.51 | 8.92 | 8.83 | 9.98 |
| $E_8$ | 8.20 | 7.48 | 8.05 | 8.69 | 7.94 | 8.55 |
| $E_9$ | 11.49 | 11.53 | 11.14 | 12.06 | 12.11 | 11.70 |
| $E_{10}$ | 14.99 | 14.56 | 14.57 | 16.22 | 15.79 | 15.80 |

or equivalently low-fidelity mesh, and mesh size equal to 5 mm, henceforth named fine mesh or equivalently high-fidelity mesh. The computational time required to model 2500 configurations with coarse mesh is about 30 min, with fine mesh is about 8 h.

Assuming the experimentally observed values of the natural frequencies as the true values, the distance between the numerical and the experimental values is the absolute error. The error of FEM model with the fine and the coarse mesh has been computed in the test points and summarized in Table 4.

It is noted that the values obtained by FEM model with coarse and fine mesh are quite close and in both cases the relative error grows at higher natural frequencies. The error remains limited becoming higher than 5% only after the tenth natural frequency.

The signed errors have been analyzed too, in order to individuate a pattern, but no patterns have been observed, which is reasonable being the natural frequencies uncorrelated.

## 4 Results

**4.1 Updated Model.** Since the accuracy of natural frequency values, obtained by FEM model with coarse and fine mesh, is similar, while the computing time largely increases using a fine mesh, the model updating have been run only with the coarse mesh model.

The model updating consists in searching for Young's modulus $E$ and density $\rho$ of the plate to move the numerical results closer to experimental values.

The model updating was conducted in DDS FEMTools.

At first, we have tried a model updating starting from the model obtained with $E = 210{,}000\ \text{N/mm}^2$ and $\rho = 7800\ \text{kg/m}^3$. The code was not able to increment the match between numerical and experimental results.

As second attempt, we have tried a model updating starting from a *bad* model obtained with $E = 300{,}000\ \text{N/mm}^2$ and $\rho = 6000\ \text{kg/m}^3$. The code was able to find a model closer to experimental results with $E = 206{,}409\ \text{N/mm}^2$ and $\rho = 8054\ \text{kg/m}^3$.

In Table 5 there is a comparison among the plate's natural frequencies obtained by the three different models: the original, the *bad*, and the updated one.

The updated model values are now very close to experimental ones. The relative errors are less than 2.3%.

Using the updated $E$ and $\rho$, the natural frequencies of the complete system, plate plus masses, have been computed again for all 2500 configurations ($x_1$, $x_2$). The relative error in test points is now less than 3.2% for all first 10 natural frequencies.

The achieved improvement is evident in Figs. 3(*a*) and 3(*b*), where the natural frequency 9 is shown, as an example.

In practical cases, the maps, obtained by the model updating, for each natural frequency and masses configuration, are those a technician should use to find the correct setup of the system. In the specific case, they allow to identify the setup to avoid having the natural frequencies at specific resonance values. The time needed to build these maps is function of the amount of configurations needed to achieve an appropriate response surface, able to give a reasonable knowledge of the dynamic system behavior, plus that needed for the initial model updating. In this case, a simplified model has been used, so the model updating was immediate, but that is not the case for complex systems.

Let us notice that, if we acquire, during the operative phase of the plant, new experimental values, it is not possible to add the information to the numerical model in order to improve it. This would be possible only if we perform a model updating using the complete system, but this means we have to perform a full optimization to find the best numerical model variables for all measured configurations, so that the complexity of the approach to build the maps for each natural frequency increases, such as the computational time and cost.

**4.2 Kriging.** The kriging model, differently by the updated model presented in Sec. 4.1 and the recursive cokriging model presented in Sec. 4.3, is built using only experimental observations, neglecting the results of the FEM analysis.

**Table 5 Natural frequencies *f* of plate obtained by three different FEM models**

| (Hz) | Experimental | $E = 210{,}000\ \text{N/mm}^2$ | $\rho = 7800\ \text{kg/m}^3$ | $E = 300{,}000\ \text{N/mm}^2$ | $\rho = 6000\ \text{kg/m}^3$ | $E = 206{,}409\ \text{N/mm}^2$ | $\rho = 8054\ \text{kg/m}^3$ |
|---|---|---|---|---|---|---|---|
| $f_1$ | 28.93 | 29.79 | | 40.60 | | 28.94 | |
| $f_2$ | 46.88 | 47.71 | | 65.02 | | 46.34 | |
| $f_3$ | 80.18 | 82.88 | | 112.95 | | 80.51 | |
| $f_4$ | 99.61 | 102.02 | | 139.03 | | 99.10 | |
| $f_5$ | 156.62 | 162.74 | | 221.78 | | 158.08 | |
| $f_6$ | 162.23 | 169.48 | | 230.96 | | 164.63 | |
| $f_7$ | 202.64 | 211.75 | | 288.57 | | 205.69 | |
| $f_8$ | 220.58 | 228.64 | | 311.59 | | 222.10 | |
| $f_9$ | 245.48 | 256.05 | | 348.94 | | 248.73 | |
| $f_{10}$ | 262.82 | 276.91 | | 377.37 | | 268.99 | |

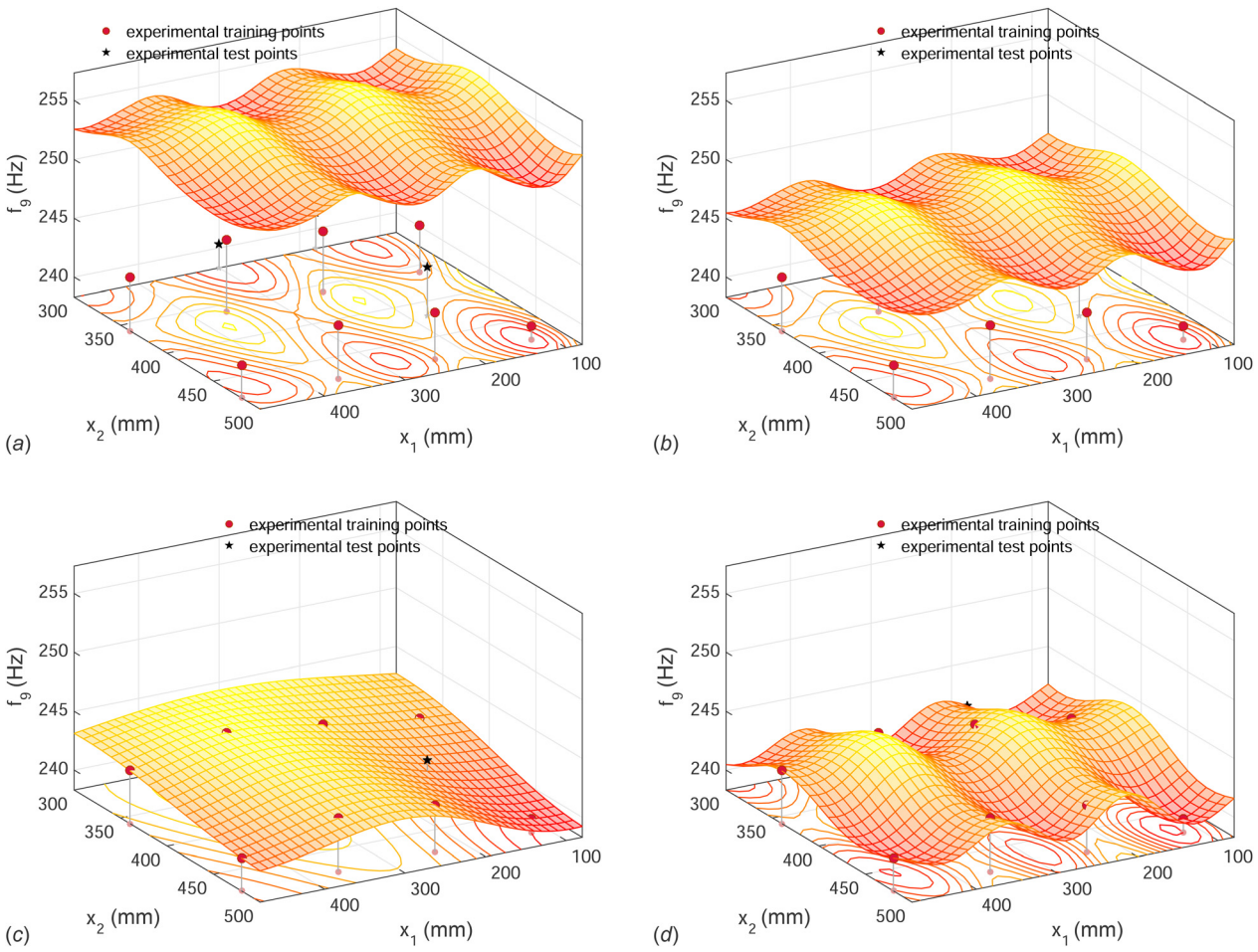


**Fig. 3 Natural frequency 9: comparison between numerical models and experimental values: (*a*) original FE model, (*b*) updated FE model, (*c*) kriging model, and (*d*) recursive cokriging model**

The kriging model has been computed using eight experimental values. The computational time needed to map the first 10 natural frequencies in 2500 configurations is about 1 min. The kriging model is a Gaussian process, so that it provides the mean and the standard deviation of each predicted value. Being a standard deviation associated with the prediction for each configuration, the confidence of the model is known. Obviously, the standard deviation is zero and the kriging model is exact at the measured configuration. This is evident both in Figs. 3(*c*) and 4(*b*). Figure 3(*c*) shows the predicted values of natural frequency 9, that is, the mean of the kriging model, which fits the experimental training points. Figure 4(*b*) shows the standard deviation of kriging model for natural frequency 9 as function of ($x_1$, $x_2$). The standard deviation is exactly 0 in correspondence of the experimental training points. The training points are not shown for clarity purposes.

Table 6 reports the absolute errors of kriging model in test points. Let us remark they are similar to those of the updated model, but the computational time and cost to build the maps for each natural frequency, varying the masses configuration, is paltry respect to that needed using the model updating.

At the same time, it is evident that some features of the function are lost. Let us underline if we acquire new experimental values, we can improve the kriging model adding the information. But, this has a cost, because the increasing of the number of observations demands higher computational cost. $N$ observations lead to an $O(N^3)$ scaling for implementations based on maximum likelihood estimation, such as the employed model.

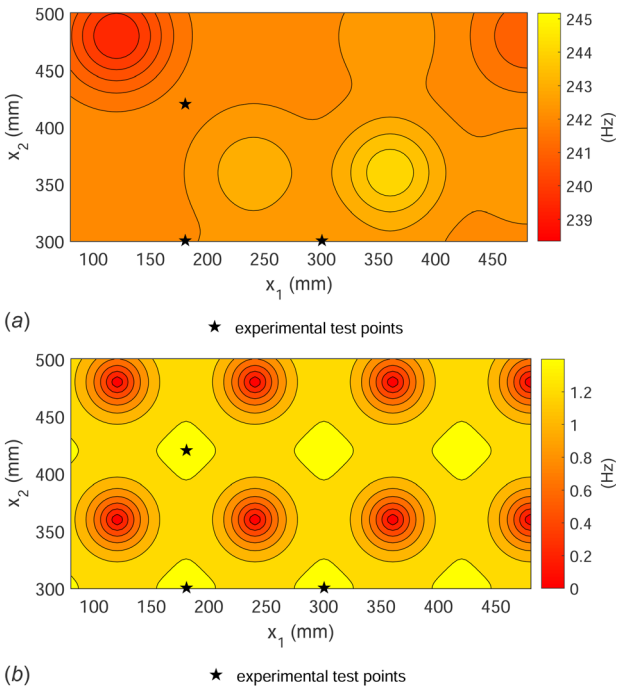


**Fig. 4 Kriging model of natural frequency 9: (*a*) mean and (*b*) standard deviation**

**Table 6 Absolute errors of updated FEM model, kriging model and recursive cokriging model respect to experimental natural frequencies in test points**

| | Updated | | | Kriging | | | Recursive cokriging | | |
|---|---|---|---|---|---|---|---|---|---|
| (Hz) | $p_1$ | $p_2$ | $p_3$ | $p_1$ | $p_2$ | $p_3$ | $p_1$ | $p_2$ | $p_3$ |
| $E_1$ | 0.06 | 0.05 | 0.07 | 0.05 | 0.24 | 0.14 | 0.00 | 0.12 | 0.02 |
| $E_2$ | 0.51 | 0.37 | 0.54 | 0.01 | 0.03 | 0.05 | 0.02 | 0.05 | 0.03 |
| $E_3$ | 0.64 | 0.41 | 0.43 | 0.28 | 1.52 | 1.44 | 0.14 | 0.14 | 0.01 |
| $E_4$ | 0.14 | 0.64 | 0.21 | 0.15 | 0.50 | 0.42 | 0.10 | 0.10 | 0.25 |
| $E_5$ | 1.99 | 3.30 | 1.18 | 2.35 | 0.08 | 5.14 | 0.30 | 1.69 | 1.70 |
| $E_6$ | 2.52 | 2.70 | 2.28 | 0.36 | 0.87 | 1.77 | 0.29 | 0.31 | 0.37 |
| $E_7$ | 3.07 | 3.04 | 3.99 | 1.52 | 0.67 | 2.74 | 1.14 | 1.40 | 0.17 |
| $E_8$ | 2.24 | 1.65 | 2.01 | 0.28 | 1.38 | 2.07 | 0.06 | 0.76 | 1.04 |
| $E_9$ | 4.89 | 4.86 | 4.62 | 2.38 | 0.94 | 3.95 | 0.00 | 0.48 | 0.89 |
| $E_{10}$ | 8.31 | 7.88 | 7.88 | 6.99 | 7.29 | 7.36 | 3.06 | 2.31 | 2.87 |

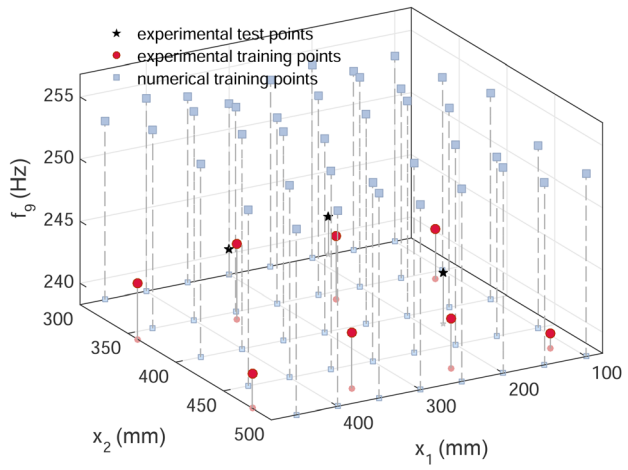


**Fig. 5 Natural frequency 9: high-fidelity and low-fidelity training points of recursive cokriging model**

**4.3 Recursive Cokriging.** The recursive cokriging model has been computed using 40 low-fidelity training points and 8 high-fidelity ones. The low-fidelity training points are computed by FEM code with coarse mesh and high-fidelity points are those experimentally observed. Figure 5 shows the training points used to model natural frequency 9, as an example.

The computational time needed to map the first 10 natural frequencies in 2500 configurations is about 3.5 min. Figure 6 shows the mean and the standard deviation of cokriging prediction for natural frequency 9 as function of $(x_1, x_2)$. Observing Figs. 6(*b*) and 4(*b*), it is evident that the standard deviation has been greatly reduced compared to kriging model which has been built using the same number of high-fidelity training points. This is because the recursive cokriging model takes into account of a considerable number of cheap low-fidelity observations, too.

Recursive cokriging model, here based on two fidelity levels but more levels could be used, is able to reduce the error in the test points (see Table 6) so that the relative error is now less than 1.2% for all first 10 natural frequencies (3.2% for updated model, 3.4% for kriging model).

The cokriging model has been computed even using observations obtained by FEM code with fine mesh instead of coarse and even using three levels (observations obtained by FEM code with coarse mesh, observations obtained by FEM code with fine mesh and experimental observations). These models are very close to that one we have presented. That is due to the fact that the numerical observations computed with coarse and fine mesh, even if they have different values, they have the same topology, so that they do not add significantly different information to final model.

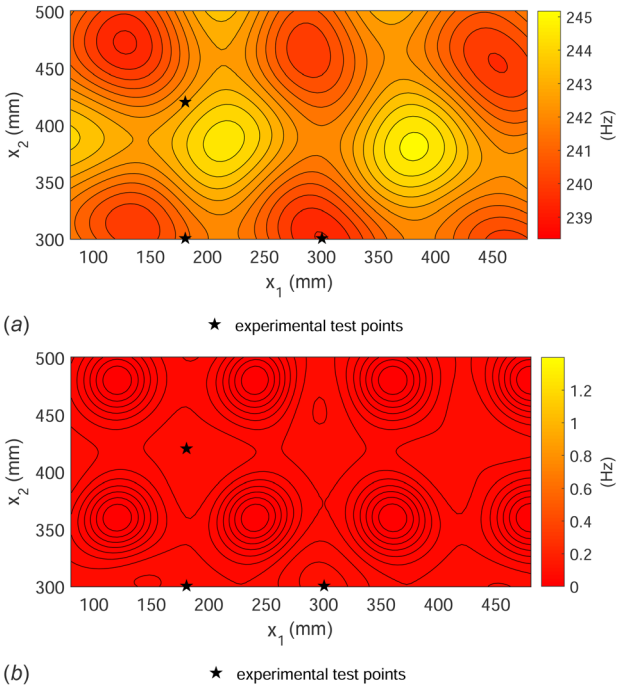


**Fig. 6 Recursive cokriging model of natural frequency 9: (*a*) mean and (*b*) standard deviation**

**Table 7 Absolute errors of recursive cokriging model in test points $p_1$ and $p_2$, moving test point $p_3$ to the training set of high-fidelity level (compare with Table 4)**

| | Recursive cokriging | |
|---|---|---|
| (*Hz*) | $p_1$ | $p_2$ |
| $E_1$ | 0.00 | 0.12 |
| $E_2$ | 0.03 | 0.05 |
| $E_3$ | 0.14 | 0.15 |
| $E_4$ | 0.14 | 0.12 |
| $E_5$ | 0.29 | 1.32 |
| $E_6$ | 0.30 | 0.42 |
| $E_7$ | 0.49 | 2.94 |
| $E_8$ | 0.34 | 0.49 |
| $E_9$ | 0.13 | 0.47 |
| $E_{10}$ | 0.86 | 0.20 |

Let us notice that, as for kriging, new experimental values, acquired during operative phase, can be added to our model in order to improve it. Thanks to recursive formulation, adding training points to the high fidelity level does not request the recalculation of all lower levels, but only of the final one. So, new information can be added at a cheap computational cost, till the number of experimental observations is less than 1000.

The benefit of adding new experimental values to recursive cokriging model is visible observing the new model, computed moving one of the test point to the training set of high-fidelity level. For example, in Table 7, there are the absolute errors of the recursive cokriging model moving the test point $p_3$ in the training set. It is remarkable that the error reduction we have obtained except for natural frequency 7 in test point $p_2$. But, even that it is not so disturbing, because, observing Figs. 7(*b*) and 7(*d*), a considerable average reduction of the standard deviation of natural frequency 7 has been obtained adding test point $p_3$ to training points.

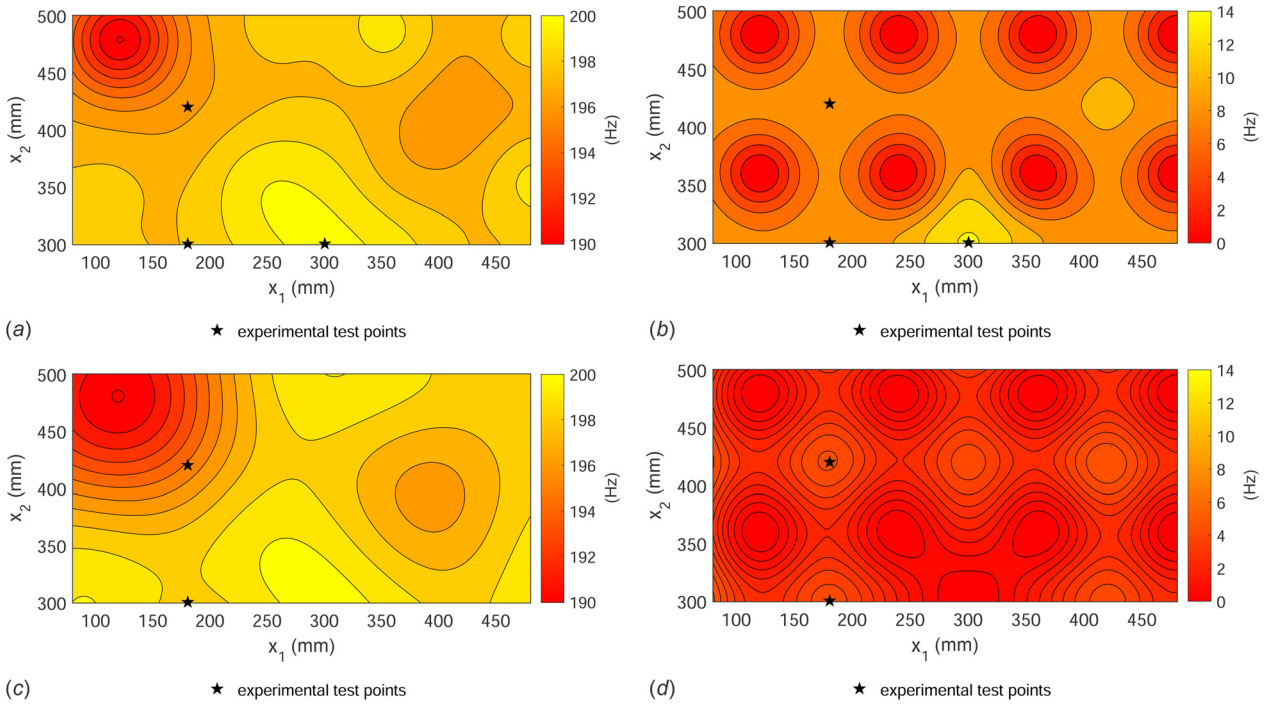


**Fig. 7 Recursive cokriging model of natural frequency 7: (*a*) mean and (*b*) standard deviation are computed using 8 high fidelity training points, (*c*) mean and (*d*) standard deviation are computed using 9 high fidelity training points**

In order to increase the confidence in the results, the recursive cokriging models have been recomputed exploiting 8 different training points among the 11 experimental observations at disposal, computing the absolute error in the remaining 3 points used for testing the models. 20 different randomly chosen combinations have been analyzed. We have not reported all the results on the paper, to not make it heavier, but they confirm what previously observed.

## 5 Application

Let us consider the system shown in Fig. 8. The system is the same as the previously described test case, on which a third mass has been added. Its position is fixed at (495 mm, 55 mm), in the referring system shown in figure, and its weight is 240 $g$. As previously, other two masses can be placed along two lines, parallel to the long side on the plate, at two fixed ordinates. Again, a system configuration is completely described by the two variables $x_1$ and $x_2$, which are the abscissas where mass 1 and mass 2 are positioned, respectively.

Let us suppose two excitation forces, with frequencies $f_{e1} = 216$ Hz and $f_{e2} = 231$ Hz, are acting on the system. We want to find the best configuration of masses 1 and 2 to assure the natural frequencies of the system are far enough from the two forcing frequencies, to avoid the resonance effects.

We compute the recursive cokriging model of the first 10 natural frequencies of the system as function of $(x_1, x_2)$. 81 training points, obtained by FEM with a coarse mesh, and 19 training points, obtained by measurements, have been used to compute the models.

The obtained recursive cokriging models have been used to point out which are the closest natural frequencies to $f_{e1}$ and $f_{e2}$, that are frequencies $f_8$ and $f_9$.

Let us name the prediction of these natural frequencies as $\hat{m}_{f_8}$ and $\hat{m}_{f_9}$ and the standard deviation of the prediction as $\hat{s}_{f_8}$ and $\hat{s}_{f_9}$. It is reasonable that the configurations $(x_1, x_2)$, where the prediction of the natural frequencies $\hat{m}_{f_8}$ and $\hat{m}_{f_9}$ are outside the intervals

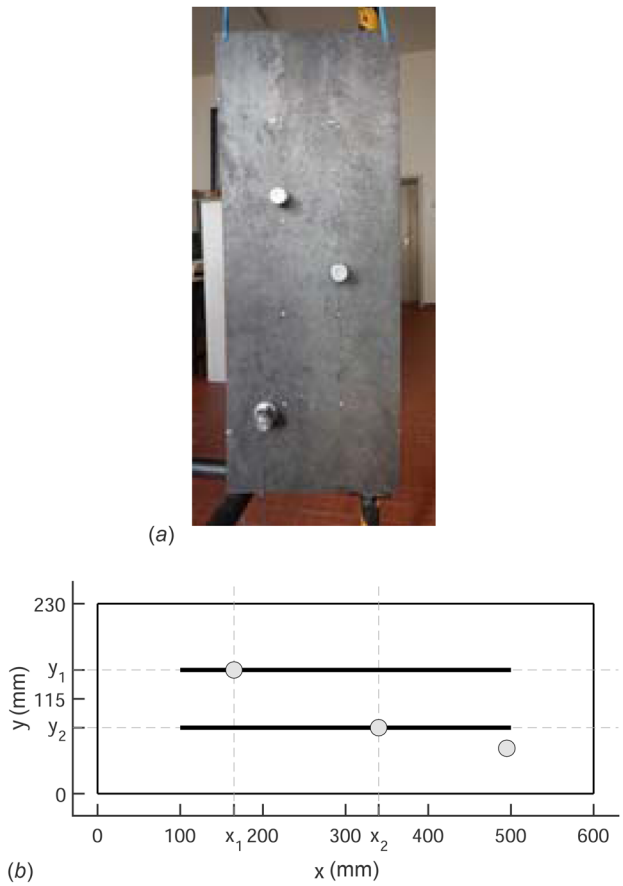


**Fig. 8 (*a*) Picture and (*b*) scheme of system to optimize (in (b) the bold lines represent the points where the two masses can be positioned)**

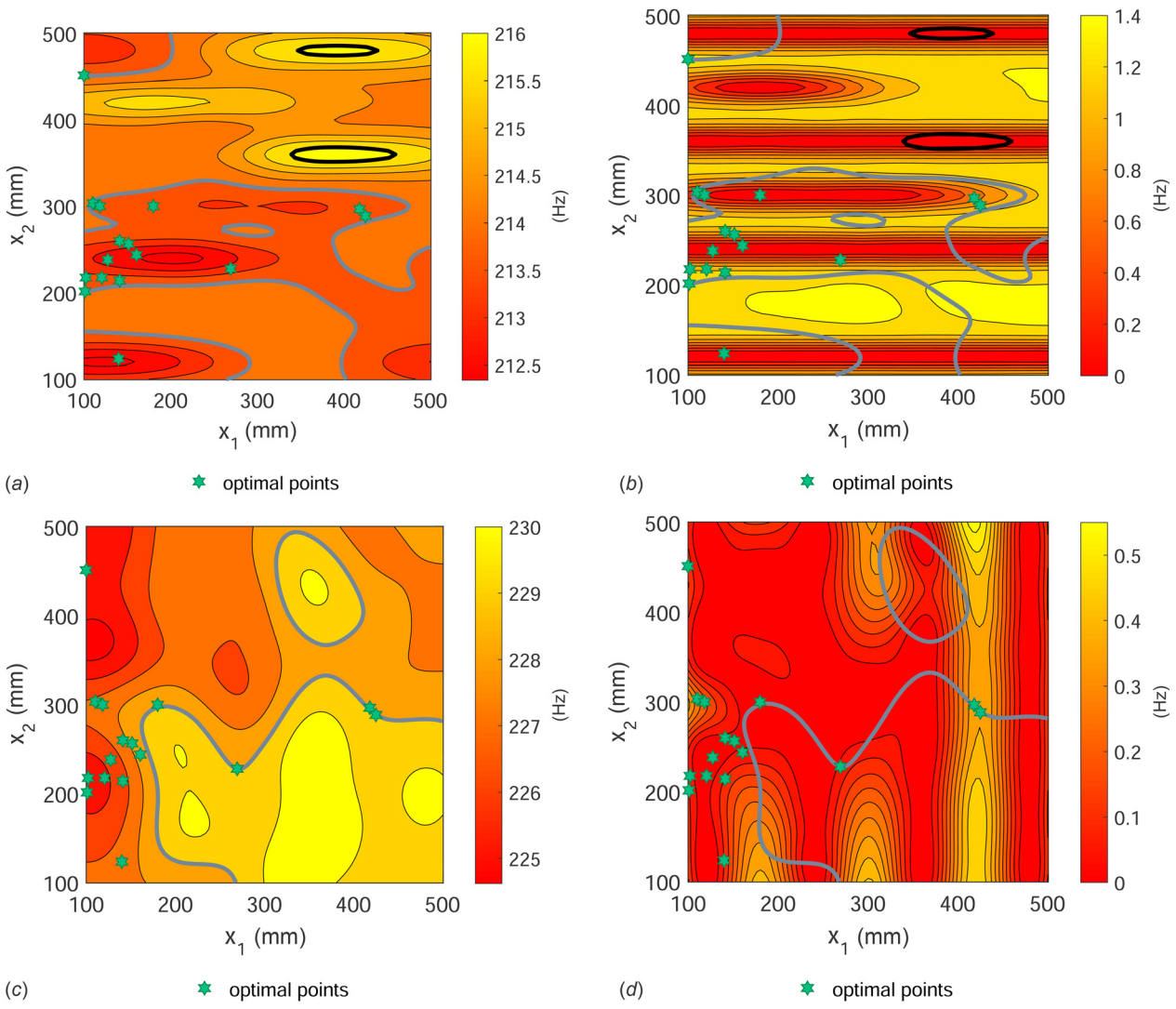


**Fig. 9 Recursive cokriging model of natural frequencies 8 an 9: (*a*) $f_8$ mean, (*b*) $f_8$ standard deviation, (*c*) $f_9$ mean, and (*d*) $f_9$ standard deviation (black line: locus of points ($x_1$, $x_2$), where the natural frequency is equal to frequency $f_{e1}$ or $f_{e2}$; gray line: locus of points ($x_1$, $x_2$), where the natural frequency is equal to frequency $f_{e1}\pm2$ Hz or $f_{e2}\pm2$ Hz)**

$f_{e1}\pm2$ Hz and $f_{e2}\pm2$ Hz, will avoid the appearance of resonance. Different intervals could also be explored.

Among all these feasible configurations, we want to find the one which guarantees, simultaneously, the maximum distances between the natural frequencies $f_8$ and $f_9$ and the exciting frequencies $f_{e1}$ and $f_{e2}$.

We use a GA algorithm to perform the optimization. The searching interval is $(x_1, x_2) \in [100, 500] \times [100, 500]$ mm$^2$. The objectives to optimize are 6

$$\max |\hat{m}_{f_8}(x_1,x_2) - f_{e1}| \tag{9}$$

$$\max |\hat{m}_{f_8}(x_1,x_2) - f_{e2}| \tag{10}$$

$$\max |\hat{m}_{f_9}(x_1,x_2) - f_{e1}| \tag{11}$$

$$\max |\hat{m}_{f_9}(x_1,x_2) - f_{e2}| \tag{12}$$

$$\min \hat{s}_{f_8}(x_1,x_2) \tag{13}$$

$$\min \hat{s}_{f_9}(x_1,x_2) \tag{14}$$

and the constrains are 4

$$(\hat{m}_{f_8}(x_1,x_2) - f_{e1})^2 > 4 \tag{15}$$

$$(\hat{m}_{f_8}(x_1,x_2) - f_{e2})^2 > 4 \tag{16}$$

$$(\hat{m}_{f_9}(x_1,x_2) - f_{e1})^2 > 4 \tag{17}$$

$$(\hat{m}_{f_9}(x_1,x_2) - f_{e2})^2 > 4. \tag{18}$$

Let us remember that the lower is the standard deviation, the higher is the probability to have performed an accurate prediction. So, the inclusion of the standard deviation of the predicted values in the optimization allows to find configurations able, not only to assure the maximum distances between the natural and the exciting frequencies but also to assure the maximum distances with the maximum reliability.

Being the optimization problem, a multi objective optimization, we have obtained a set of optimal configurations, shown in Fig. 9 (the values are reported in Appendix C).

It is evident how the best configurations, named as optimal points, lay all in the zone, of the nonlinear surface maps, where

the difference to the excitation frequencies are the highest and the standard deviations are minimal.

## 6 Conclusion

Engineers and technicians often have to identify the correct setup of a plant, during the operative phase. To avoid the attempts and common sense practice, a map of the process parameters must be built on the setup variables. There are methods which exploit both experimental and numerical observations, to build this map, such as the model updating of a FEM model and the multifidelity response surfaces. These allow to reduce the number of measurements and experiments.

In this paper, we have compared the updated model, kriging model and recursive cokriging model, analyzing the advantages and disadvantages of the approaches by a practical example. The process variables to map are the natural frequencies of a system made up by a plate and two masses whose positions on the plate correspond to different setup configurations. Thanks to the proposed recursive cokriging, for each masses' positions, we are capable to predict the resonance frequencies' values with extremely low relative errors.

The recursive cokriging model has shown to be more computational cost-effective and accurate than the updated model, and even more precise of the kriging model on which recursive cokriging method grounds. It is worthwhile noticing that the response surfaces do not allow to identify the physical parameters of the system, such as the Young's modulus and the density of the plate. Such issue can be faced only by model updating, which search for the physical parameters that move numerical analysis results closer to measured data.

In our test case, we obtained the response surface in the model updating case out of 2500 numerical simulations, while in the recursive cokriging case with just 40 computations. The resources' saving is evident.

The recursive cokriging model can be definitely used to perform the optimization of process parameters, as shown in Sec. 5.

Moreover recursive cokriging model can be easily updated with new experimental observations collected during the functioning of the plant. This means that we can also monitor the process parameters to detect variations caused by wear and malfunction.

Nevertheless, we are aware that recursive cokriging has some limitations: it performs well only for smooth phenomena and the higher the number of the system variables is, the higher is the number of the observations needed to have an accurate prediction. This leads to an increase in computational time, as already underlined in Sec. 4.3.

In our opinion, the strong point of the approach is its recursive framework to exploit multifidelity data. We believe that the same recursive scheme could be exploited to model highly nonlinear phenomena, as it will be shown in a following paper:

## Appendix A: Kriging

The joint distribution of $Z(\mathbf{x})$ and $\mathbf{Z}^{(n)}$ is given by

$$\begin{pmatrix} Z(\mathbf{x}) \\ \mathbf{Z}^{(n)} \end{pmatrix} \sim \mathcal{N}\left( \begin{pmatrix} \mathbf{h}(\mathbf{x})\boldsymbol{\beta} \\ \mathbf{H}\boldsymbol{\beta} \end{pmatrix}, \sigma^2 \begin{pmatrix} 1 & \mathbf{r}^{\mathrm{T}}(\mathbf{x}) \\ \mathbf{r}(\mathbf{x}) & \mathbf{R} \end{pmatrix} \right) \tag{A1}$$

where

$$\mathbf{H} = \begin{pmatrix} h_1(\mathbf{x}_1) & \dots & h_p(\mathbf{x}_1) \\ \vdots & \ddots & \vdots \\ h_1(\mathbf{x}_n) & \dots & h_p(\mathbf{x}_n) \end{pmatrix} \tag{A2}$$

is the $n \times p$ model matrix

$$\mathbf{R} = \begin{pmatrix} r(\mathbf{x}_1, \mathbf{x}_1) & \dots & r(\mathbf{x}_1, \mathbf{x}_n) \\ \vdots & \ddots & \vdots \\ r(\mathbf{x}_n, \mathbf{x}_1) & \dots & r(\mathbf{x}_n, \mathbf{x}_n) \end{pmatrix} \tag{A3}$$

is the $n \times n$ correlation matrix between the observations $\mathbf{Z}^{(n)}$ and

$$\mathbf{r}(\mathbf{x}) = \begin{pmatrix} r(\mathbf{x}, \mathbf{x}_1) \\ \vdots \\ r(\mathbf{x}, \mathbf{x}_n) \end{pmatrix} \tag{A4}$$

is the $n \times 1$ correlation vector between $Z(\mathbf{x})$ and the observations $\mathbf{Z}^{(n)}$.

## Appendix B: Recursive Cokriging

The joint distribution of $Z_t(\mathbf{x})$ and $\mathbf{Z}^{(t)}$ is given by

$$\begin{pmatrix} Z_t(\mathbf{x}) \\ \mathbf{Z}^{(t)} \end{pmatrix} \sim \mathcal{N}\left( \begin{pmatrix} \mathbf{f}_t(\mathbf{x})\boldsymbol{\beta}_t + \rho_{t-1}(\mathbf{x})\hat{m}_{Z_{t-1}}(\mathbf{x}) \\ \mathbf{F}_t\boldsymbol{\beta}_t + \rho_{t-1}(\mathcal{D}_t) \odot \mathbf{z}_{t-1}(\mathcal{D}_t) \end{pmatrix}, \right.$$
$$\left. \rho^2_{t-1}(\mathbf{x})\hat{s}^2_{Z_{t-1}}(\mathbf{x}) \begin{pmatrix} \mathbf{1} & \mathbf{0} \\ \mathbf{0} & \mathbf{0} \end{pmatrix} + \sigma^2_t \begin{pmatrix} 1 & \mathbf{r}^T_t(\mathbf{x}) \\ \mathbf{r}_t(\mathbf{x}) & \mathbf{R}_t \end{pmatrix} \right) \tag{B1}$$

where $\mathcal{D}_t = (\mathbf{x}^{(t)}_1, \dots, \mathbf{x}^{(t)}_{n_t})^{\mathrm{T}}$

$$\mathbf{F}_t = \begin{pmatrix} f_1(\mathbf{x}^{(t)}_1) & \dots & f_{p_t}(\mathbf{x}^{(t)}_1) \\ \vdots & \ddots & \vdots \\ f_1(\mathbf{x}^{(t)}_{n_t}) & \dots & f_{p_t}(\mathbf{x}^{(t)}_{n_t}) \end{pmatrix} \tag{B2}$$

is the $n_t \times p_t$ experience matrix

$$\mathbf{R}_t = \begin{pmatrix} r_t(\mathbf{x}^{(t)}_1, \mathbf{x}^{(t)}_1) & \dots & r_t(\mathbf{x}^{(t)}_1, \mathbf{x}^{(t)}_{n_t}) \\ \vdots & \ddots & \vdots \\ r_t(\mathbf{x}^{(t)}_{n_t}, \mathbf{x}^{(t)}_1) & \dots & r_t(\mathbf{x}^{(t)}_{n_t}, \mathbf{x}^{(t)}_{n_t}) \end{pmatrix} \tag{B3}$$

is the $n_t \times n_t$ correlation matrix between the observations $\mathbf{Z}^{(t)}$ and

$$\mathbf{r}_t(\mathbf{x}) = \begin{pmatrix} r_t(\mathbf{x}, \mathbf{x}^{(t)}_1) \\ \vdots \\ r_t(\mathbf{x}, \mathbf{x}^{(t)}_{n_t}) \end{pmatrix} \tag{B4}$$

is the $n_t \times 1$ correlation vector between $Z_t(\mathbf{x})$ and the observations $\mathbf{Z}^{(t)}$.

**Table 8 Optimal configurations**

| | | $f_8$ (Hz) | | $f_9$ (Hz) | |
|---|---|---|---|---|---|
| $x_1$ (mm) | $x_2$ (mm) | Mean | Std. dev. | Mean | Std. dev. |
| 100 | 451 | 213.98 | 1.29 | 225.75 | 0.13 |
| 101 | 201 | 214.00 | 1.39 | 225.65 | 0.10 |
| 102 | 218 | 213.66 | 1.14 | 225.55 | 0.07 |
| 110 | 304 | 213.99 | 0.33 | 227.14 | 0.26 |
| 118 | 300 | 213.95 | 0.21 | 227.38 | 0.21 |
| 120 | 218 | 213.63 | 1.13 | 225.81 | 0.02 |
| 127 | 238 | 212.83 | 0.02 | 226.40 | 0.01 |
| 140 | 124 | 212.48 | 0.08 | 227.48 | 0.11 |
| 141 | 214 | 213.79 | 1.25 | 226.67 | 0.10 |
| 141 | 260 | 213.51 | 1.04 | 227.78 | 0.04 |
| 151 | 257 | 213.30 | 0.88 | 228.23 | 0.04 |
| 160 | 244 | 212.58 | 0.09 | 228.43 | 0.06 |
| 180 | 300 | 213.75 | 0.00 | 228.88 | 0.00 |
| 269 | 228 | 213.22 | 0.57 | 229.00 | 0.06 |
| 418 | 297 | 213.73 | 0.71 | 228.96 | 0.38 |
| 425 | 289 | 213.87 | 0.98 | 229.00 | 0.40 |

## Appendix C: Optimal Configurations

The set of optimal configurations $(x_1, x_2)$ is reported in Table 8, together with the corresponding mean and standard deviation of recursive cokriging model for natural frequencies 8 and 9.

## References


[1] Fernandez-Godino, M. G., Park, C., Kim, N.-H., and Haftka, R. T., 2017, "Review of Multi-Fidelity Models," e-print arXiv: 1609.07196.

[2] Friswell, M. I., and Mottershead, J. E., 1995, *Finite Element Model Updating in Structural Dynamics. Solid Mechanics and Its Applications*, Kluwer Academic Publishers Group, Dordrecht, The Netherlands.

[3] Lucifredi, A., Mazzieri, C., and Rossi, M., 2000, "Application of Multiregressive Linear Models, Dynamic Kriging Models and Neural Network Models to Predictive Maintenance of Hydroelectric Power Systems," Mech. Syst. Signal Process., **14**(3), pp. 471–494.

[4] Liu, X., Li, M., and Xu, M., 2016, "Kriging Assisted On-Line Torque Calculation for Brushless DC Motors Used in Electric Vehicles," Int. J Automot. Technol., **17**(1), pp. 153–164.

[5] Krige, D. G., 1951, "A Statistical Approach to Some Basic Mine Valuation Problems on the Witwatersrand," J. Southern Afr. Inst. Min. Metall., **52**(6), pp. 119–139.

[6] Matheron, G., 1963, "Principles of Geostatistics," Econ. Geol., **58**(8), pp. 1246–1266.

[7] Sacks, J., Welch, W., J., Toby, M., and Wynn, H. P., 1989, "Design and Analysis of Computer Experiments," Stat. Sci., **4**(4), pp. 409–423.

[8] Kennedy, M. C., and O'Hagan, A., 2000, "Predicting the Output From a Complex Computer Code When Fast Approximations are Available," Biometrika, **87**(1), pp. 1–13.

[9] Gratiét, L. L., and Cannamela, C., 2015, "Kriging-Based Sequential Design Strategies Using Fast Cross-Validation Techniques With Extensions to Multi-Fidelity Computer Codes," Technometrics, **57**(3), pp. 418–427.

[10] Gratiét, L. L., 2012, "Bayesian Analysis of Hierarchical Multi-Fidelity Codes," SIAM J. Uncertainty Quantif., **1**(1), pp. 244–269.

[11] Gratiét, L. L., 2013, "Multi-Fidelity Gaussian Process Regression for Computer Experiments," Ph.D. thesis, University of Paris VII Denis-Diderot, Paris, France.